CO2-EMISSION REDUCTION BY MEANS OF ENHANCEMENT OF THE THERMAL CONVERSION EFFICIENCY OF ICE CYCLES

Gheorghiu, Victor
Department of Mechanical Engineering,
Hamburg University of Applied Sciences,
Berliner Tor 21, 20099 Hamburg, Germany
E-mail: victor.gheorghiu@haw-hamburg.de

ABSTRACT

Most recent implementations of the Atkinson cycle are not ideal from the point of view of thermal conversion efficiency (TCE). For example, Toyota has put a gasoline engine in its Prius II which should achieve high efficiency by using a modified Atkinson cycle based on variable intake valve timing management. Firstly, this implementation of the Atkinson cycle is not the ideal solution because some of the air is first sucked from the intake manifold into the cylinder and subsequently returned back there. Consequently, the oscillating air stream reduces the thermal conversion efficiency of this cycle to a considerable extent. Secondly, this implementation of the Atkinson cycle only reaches low levels of indicated mean pressure (IMEP) and, thirdly, it is not suitable for part load engine operating points (EOP) because of the lower TCE. For these reasons, this implementation of the Atkinson cycle is only suitable for hybrid vehicles, where the engine - because it is not directly linked mechanically to the wheels - works only in its best EOP.

This paper analyzes the losses in TCE of internal combustion engine (ICE) - especially for the Atkinson cycles - in detail, and a proposal is made for their reduction for aspirated and especially for high pressure supercharged engines.

INTRODUCTION

The principal purpose of this investigation is to discover new ways of implementing the Atkinson cycle, which simultaneously enable the enhancement of TCE and IMEP under stoichiometric air-fuel ratio (AFR) and lower pressure and temperature peaks during the cycle.

In conventional engines, as the volumetric compression and expansion strokes are virtually identical and the cylinder filling is complete, the effective compression ratio and the effective expansion ratio are basically identical, as shown on the left side of Fig. 1, for the modified Seiliger cycle (an ideal model of engine cycles). In the classic Seiliger cycle [2], or limited pressure cycle [1], the heat is released by constant volume (V) and constant pressure (p). For this reason, this cycle is referred to here as the V,p cycle. In the modified Seiliger cycle (see left side of Fig. 1), the heat is released by constant volume, constant pressure and constant temperature and, accordingly, this cycle can be referred to as the V,p,T cycle or V,p,T model. In this way, it becomes possible to generate ideal cycles which model the real ICE cycles more accurately by observing their mechanical and thermal limits. In the Atkinson cycle (see right side of Fig. 1), the effective compression stroke is shorter and the effective compression ratio is higher than those of the Seiliger cycle, meaning that the pressure at the end of the compression strokes reaches the same level in both cycles. In this case, the Atkinson cycle has a higher TCE than the Seiliger cycle.

1. The following operations are common (see [1], [2]) in order to increase the TCE of the Seiliger cycle:

2. 1. Increasing the effective volumetric compression ratio (VCR).

3. 2. Shortening the effective compression stroke, for example by delaying intake valve closing.

4. 3. Completing the effective expansion stroke, for example by delaying the exhaust valve opening.

5. 4. Enhancement of turbo charging level for a concurrent increase in TCE and indicated mean pressure (IMEP).

In conclusion, these ways for increasing the TCE of the classic Seiliger cycle (marked by arrows on the left side of Figure 1) lead to both aspirated and turbocharged engines from Seiliger to Atkinson cycle and result in the following implications, limitations and restrictions:

The first and fourth ways lead to higher pressure and temperature peaks during the cycle, which increase the thermal and mechanical strain of engine parts. The occurrence of knocking is a frequent outcome in the case of gasoline engines. The high temperature favours the production of NOx in the cylinders of both SI and Diesel engines. The second way leads to a decreased mass of retained gas in the cylinder, especially in the case of aspirated engines.

As a consequence, the IMEP only achieves low levels, and engines with a higher displacement are necessary, the mechanical losses rise, and, finally, the increase in TCE is lost. The third way leads to engines with large displacement and, consequently, with higher mechanical losses when the volumetric expansion stroke increases while the compression stroke remains unchanged.
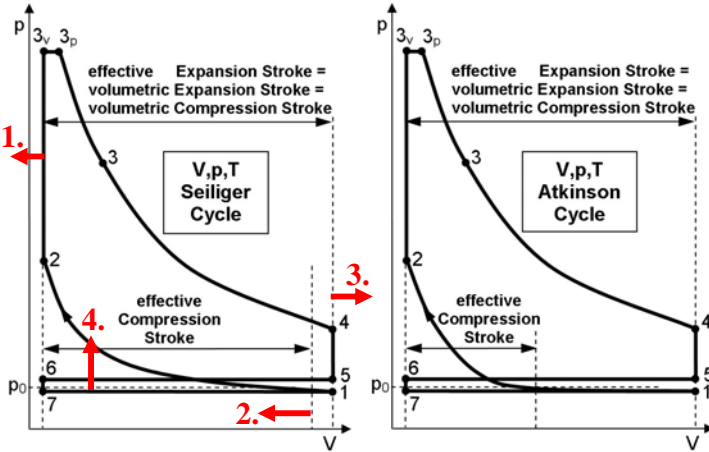

Figure 1. Schematic Pressure-Volume diagrams of classic four-stroke Seiliger and Atkinson cycle. The ways for TCE increasing are marked by arrows and lead from Seiliger to Atkinson cycle

1. ATKINSON CYCLE IMPLEMENTATIONS TO ICE WITH CLASSIC CRANKSHAFT DRIVE

1.1 Analysis of Atkinson cycle implementation for aspirated ICE

During the last few years the market share of hybrid vehicles, most of them using Spark Ignition (SI) engines, has steadily increased. For example, Toyota [3] uses a SI engine in its Prius II which attempts to achieve high efficiency by using an Atkinson cycle as shown on the right side of Figure 1. In this implementation of the Atkinson cycle the intake valve is kept open for a large part of the compression stroke, and the volumetric compression ratio is enhanced. Consequently, in the initial stage of the compression stroke (when the piston begins to ascend), some of the air that had entered the cylinder is returned to the intake manifold, in effect delaying the start of compression [3]. In this way, the expansion ratio is increased without raising the effective compression ratio. Sophisticated variable valve timing is used to carefully adjust the intake valve timing to operating conditions in order to obtain maximum efficiency. Many variants of this implementation of the Atkinson cycle were evaluated in detail in [4]. For this analysis, we have used the simulation method and tool presented in [5] and [6]. In order to eliminate the influence of the heat exchange between the compared variants, which is difficult to control, the cylinder is henceforth basically treated as adiabatic.

Figure 2 presents the indicated fuel conversion efficiency (IFCE) above the crank angle (CA) for this Atkinson cycle implementation (red dashed curve) and for the Seiliger cycle (standard variant or **SV**). The Atkinson cycle is derived from the **SV** by means of a 100°CA delay in the intake valve closing

(**ic**) and an increase of the VCR by 90%. This implementation will be labelled henceforth as the second variant or 2V.

The pushing out of residual gases during the exhaust stroke consumes more piston work in the Atkinson cycle (see A areas in Fig. 2 and 4) due to lower pressure at the exhaust valve opening (see **eo** positions in Fig. 4), meaning that the cylinder emptying is sluggish. The oscillating air stream from and to the intake manifold through the intake valve port (see Fig. 5) significantly reduces the IFCE (see B areas in Fig. 2 and 5) of the cycle. Although the compression work in this 2V Atkinson cycle implementation is greater (because of the 90% increase of VCR; see C area of Fig. 2), the increased VCR shows a very positive effect during the expansion stroke so that, finally, the IFCE level of the Seiliger cycle is reached.
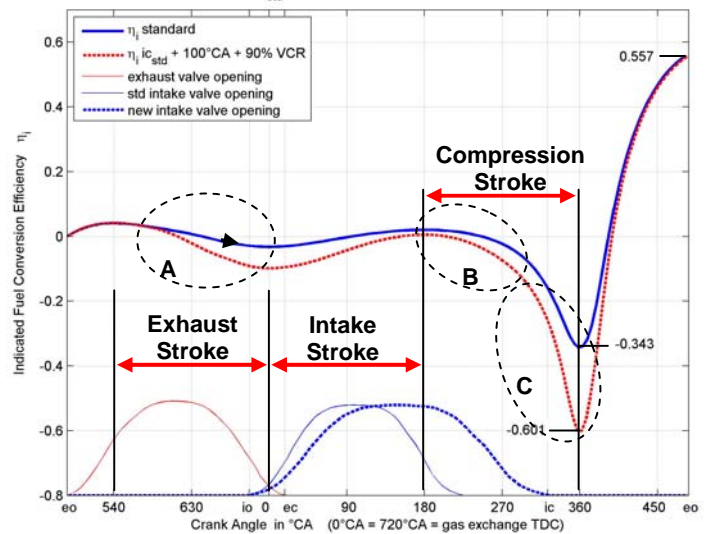

Figure 2. IFCE-CA diagrams of classic Seiliger and **2V** Atkinson cycles
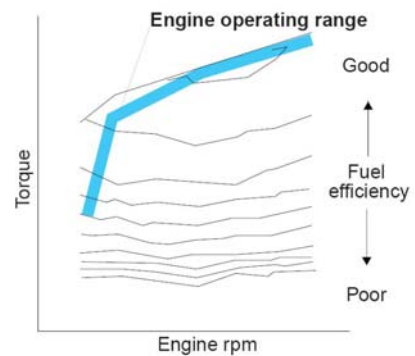

Figure 3. Engine operating range by Toyota Prius II [3]

It can therefore be concluded that the IFCE gain of this kind of Atkinson cycle implementation is modest and largely dependent on the fine-tuning of all parameters (valve timing etc.) compared to the complexity of such variable valve management. In addition, the specific power of the engine is low because of the lower retained mass of fresh change in the cylinder before compression. This means a relatively large (due

to the large displacement) and heavy engine is needed to power the vehicle. Most of the IFCE improvement in the case of Prius II is obtained by means of sifting the EOP in areas with greater IFCE (see Fig. 3). For these reasons, this implementation of the Atkinson cycle is suitable only for hybrid vehicles, where the engine - because it is not directly linked mechanically to the wheels - works only in its best operating range (see Fig. 3).
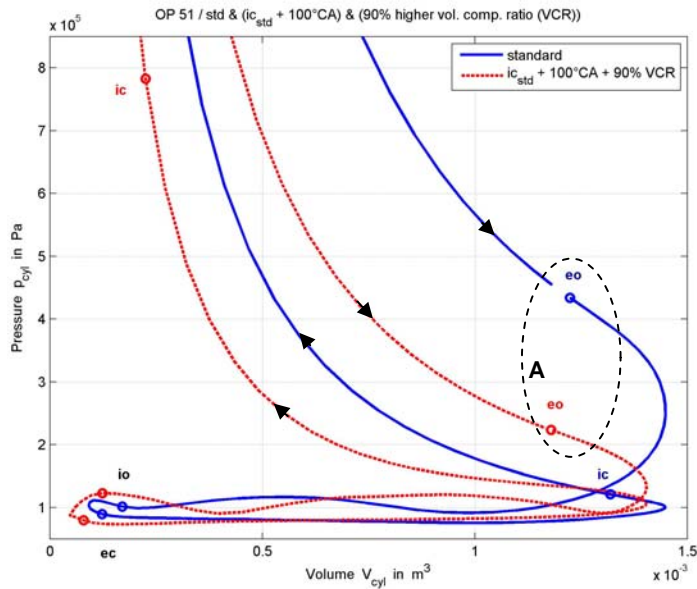

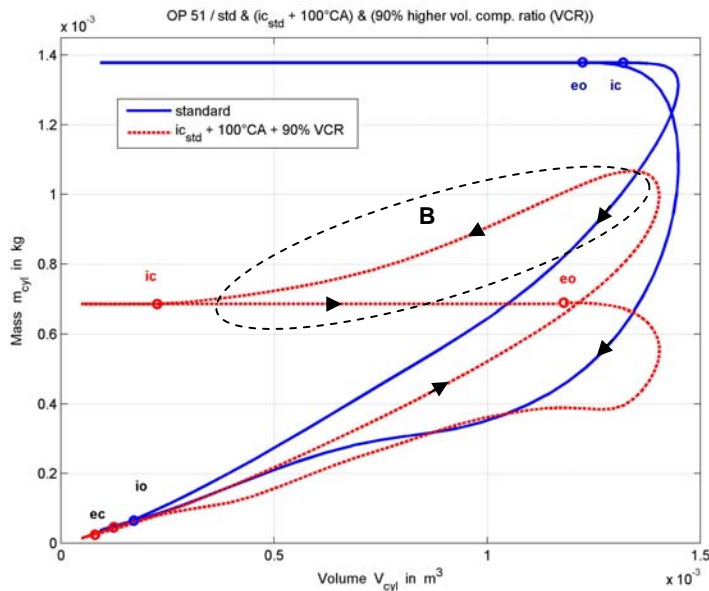**Figure 4.** Pressure-Volume diagrams of classic Seiliger and Atkinson cycles

Figure 5. Gas Mass-Volume diagrams of classic Seiliger and Atkinson cycles

1.2 Analysis of classic Atkinson cycle implementation for supercharged ICE = 1V-TC

First, the commonly used practice of concomitant suction delaying and an increase in boost pressure is analyzed. The number of parameters influencing the TCE of supercharged engines becomes much higher compared to aspirated engines. As a result, the effort to achieve combinations of parameters which maximize the TCE of such engine cycles becomes much greater.
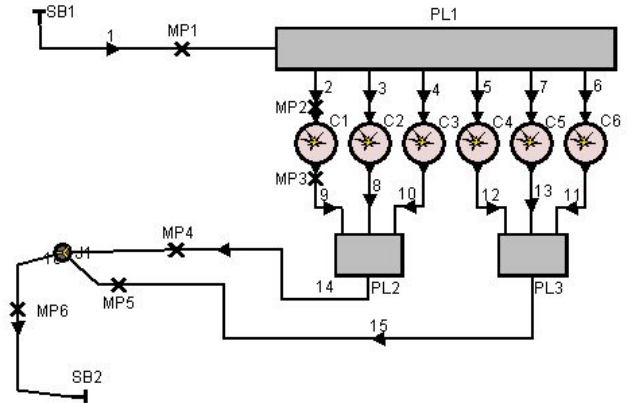

Figure 6. Simple BOOST model of a supercharged 6-cylinder diesel engine

The simulation tool used here is the BOOST®, from AVL Co. The BOOST model used for the following implementations is presented in Figure 5, where the six cylinders of the modelled engine are identical. The following options were selected for the BOOST models of the Seiliger and Atkinson cycles:

- The goal is to reach the greatest possible TCE and the indicated mean pressure at the same time, without exceeding given mechanical and thermal limits.
- The VCR for both cycles is kept identical.
- The heat transfer to the cooling system is switched off in order to enable an easier comparison between cycles and variants, as done previously in [8].
- The heat release function is modelled with the help of a simple Vibe function (identical for all simulations).
- The mechanical and thermal limits are kept identical (ca. 210 bar respectively 2,050 K) in both cycles and all of the simulation variants, as done previously in [8].
- In order to reach the same limits for pressure and temperature in both cycles, the charge pressure p_C is adjusted accordingly.
- The air-fuel ratio (λ or AFR) is kept identical in order to compare the cycles using the same load.
- The charge temperature is kept identical for all simulations ($T_C = 350$ K), as done previously in [8].
- The supercharging level is simulated by setting the state of the boundary element SB1 and the pressure before the turbine by setting the state of the boundary element SB2 (see Fig. 6). In this instance, the turbocharger and the intercooler are no longer required to be modelled in detail

and, in addition, the comparability is assured between various simulations for both cycles.

- The parameters compared here are TCE (η_{th}), IMEP (p_i), retained mass in cylinder (m_a) and pressure (p_{ic}), and also the temperature (T_{ic}) when the intake valve closes (**ic**) in both cycles.

the mechanical and thermal limitations, when very high pressure supercharging is used for an engine with classic crank drive, implies a diminishing of TCE performance.

Figure 8. Temperature – Volume Diagram of Seiliger (standard) and **1V-TC** Atkinson Cycles
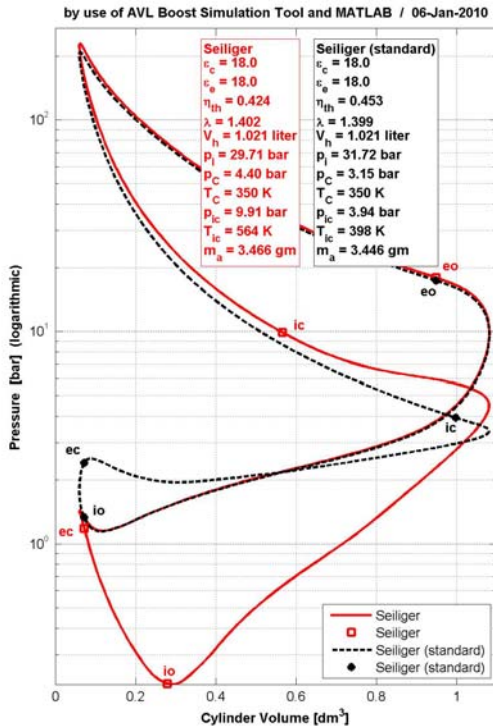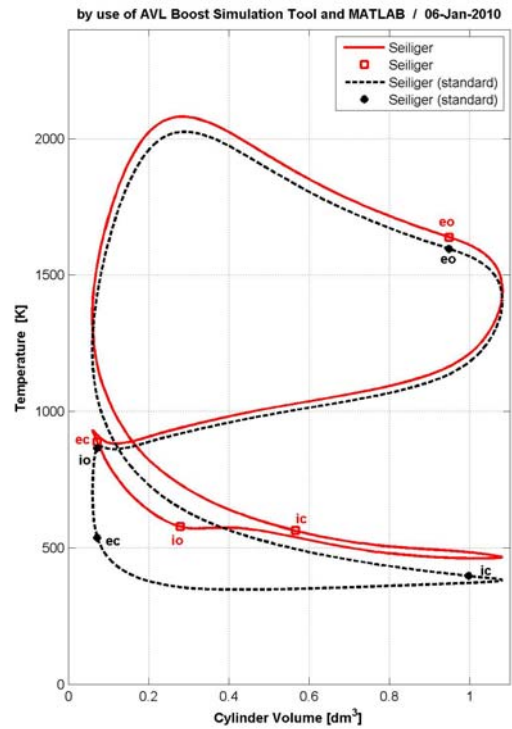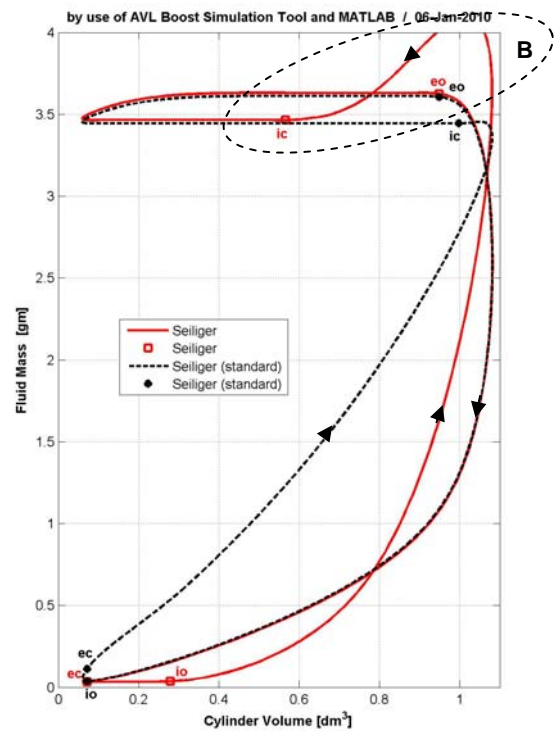

Figure 7. Pressure (logarithmic) – Volume Diagram of Seiliger (standard) and Atkinson (Seiliger Cycle with 60°CA Delayed Suction = **1V-TC**) Cycles

The simulation results for this Atkinson cycle implementation, where the intake valve closing is 60°CA delayed, are presented in Figures 7 to 10. Due to the delay in suction, the gas exchange processes are very different from the standard version of the Seiliger cycle (see Fig. 7 to 9). The boost in pressure is increased by the same filling rate of the cylinder (see Fig. 9) to achieve nearly the same IMEP.

At the beginning of the intake stroke, the pressure in the cylinder falls off significantly because the intake valve is not yet open at this time (see Fig. 7). The piston work rate is therefore lower than in the standard version (s. **A** area in Fig. 10). Toward the end of suction, when the return flow is carried to the inlet pipe (see **B** area in Fig. 9), the piston work rate is again lower than in the standard version (see **B** area in Fig. 10).

In short, although the boost pressure is 40% higher in this Atkinson cycle implementation, TCE and IMEP are 6% less than in the standard version of the Seiliger cycle. For these reasons, a new approach is needed to implement the Atkinson cycle with a normal crankshaft drive.

As a next step, a test should be done to determine the TCE improvement potential of an engine where a very high pressure supercharging and a high value of the VCR are used simultaneously. The usual reduction of the VCR for meeting

Figure 9. Fluid Mass - Volume Diagrams of Seiliger (standard) and **1V-TC** Atkinson Cycles
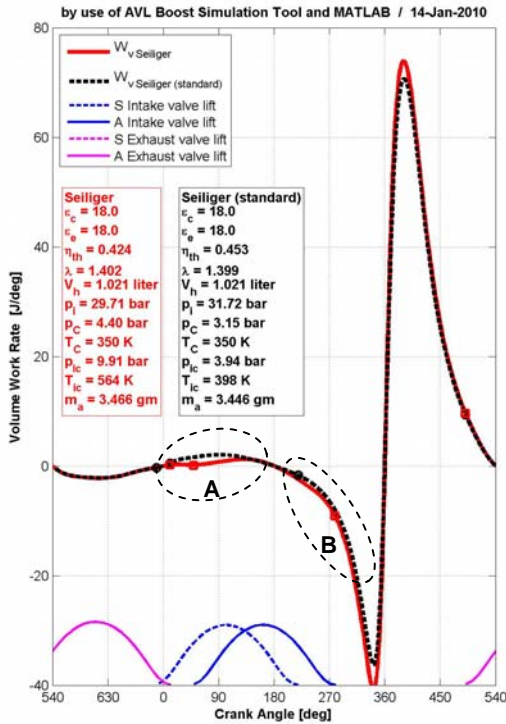
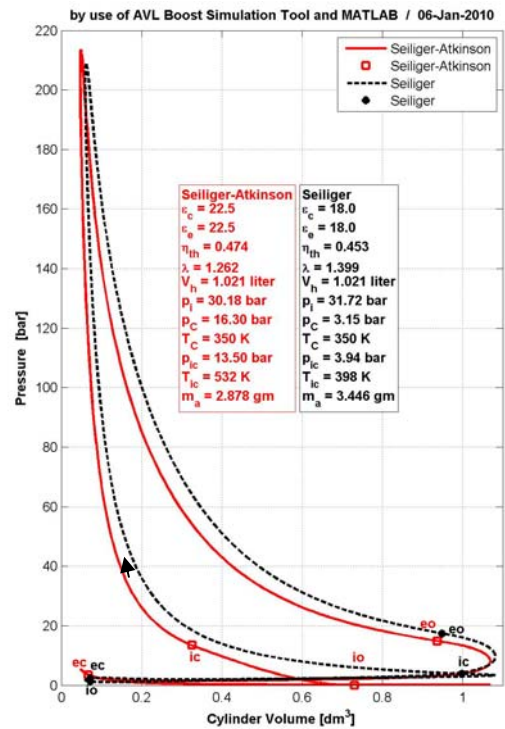**Figure 10.** Piston Work Rate - Crank Angle Diagram of Seiliger (standard) and **1V-TC** Atkinson Cycles

1.3 Analysis of an Atkinson cycle implementation to ICE with very high charge pressure = 2V-TC

In this implementation of the Atkinson cycles (labeled in Figures 11 to 14 as Seiliger-Atkinson), the suction is much more delayed and a very high charge pressure (of more than 16 bars) is taken into consideration. Due to the delayed suction less mass is aspirated into cylinder (see Fig. 13, bottom diagram). For improving the indicated TCE of the Atkinson cycle, the VCR is increased by 22% referred to the standard Seiliger cycle.

Special characteristics of the **2V-TC** Atkinson cycle implementation are: a) the rest gases are expanded during suction stroke and then compressed, as in the Miller cycle [7] and b) the suction of fresh charge starts first, after the full completion of the suction in Seiliger cycle, and takes a very short time.

Unfortunately, in order to achieve the same maximum values of pressure and temperature on both cycles at virtually the same IMEP, the AFR must be adapted in this case. The placement of the combustion phase on the cycle is identical to the standard Seiliger cycle (see Fig 13, top diagram). Simultaneous matching of all the parameters (i.e. maximum values of pressure and temperature, IMEP and AFR) is very difficult and time- consuming to achieve. The difference between the AFR values of both cycles is quite low and for this reason the EOP can be deemed to correspond to full load in both cycles.

The retained fresh charge mass into cylinder is much lower in the **2V-TC** Atkinson cycle (see Figure 13). During exhaust stroke, there are no major differences in TCE between the cycles (see Figure 14).
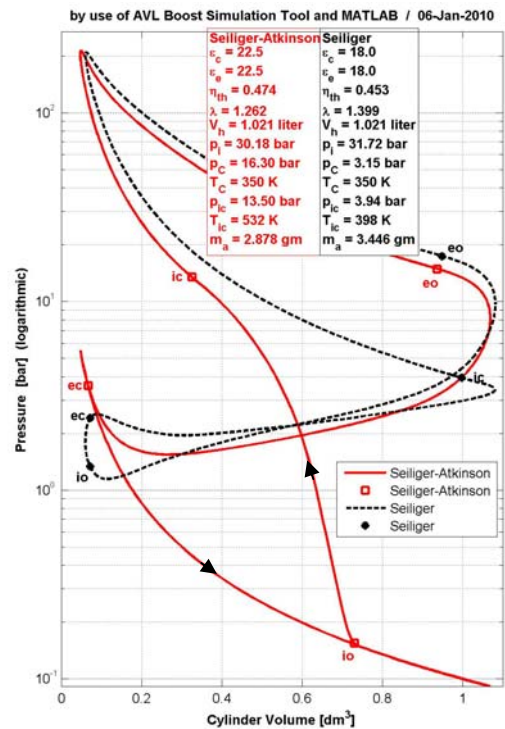

Figure 11. Pressure – Volume Diagrams of standard Seiliger and **2V-TC** Atkinson Cycles

Figure 12. Pressure (logarithmic) – Volume Diagrams of standard Seiliger and **2V-TC** Atkinson Cycles
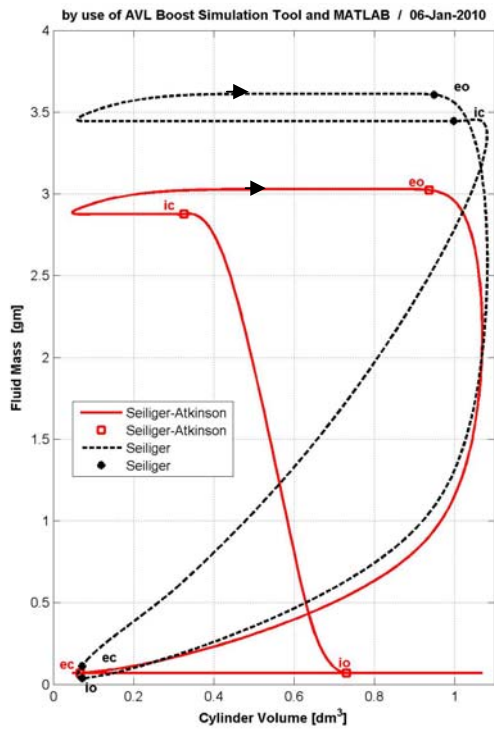
Figure 13. Fluid Mass – Volume Diagrams of standard Seiliger and **2V-TC** Atkinson Cycles
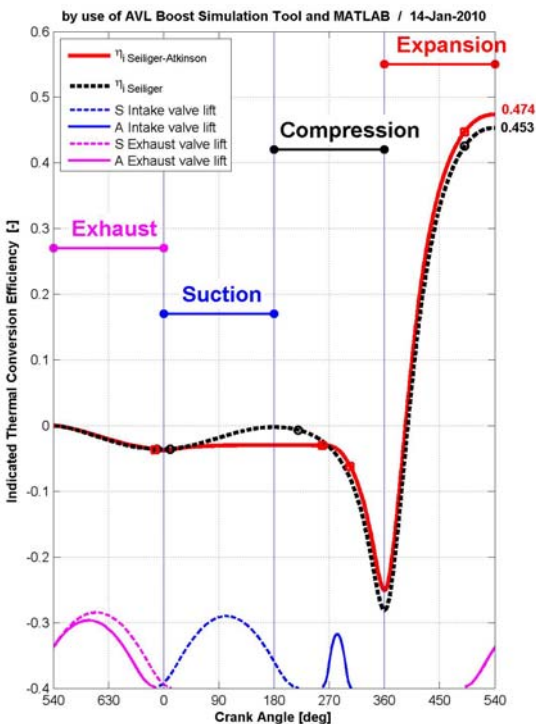

Figure 14. TCE – Crank Angle Diagrams of standard Seiliger and **2V-TC** Atkinson Cycles

The major impact of the decrease in compression work in the Atkinson cycle can be seen clearly after the closing of the

intake valve. In short, this implementation of the Atkinson cycle is somewhat more efficient than the Seiliger cycle. The improvement in TCE for the **2V-TC** Atkinson cycle, compared to the Seiliger cycle, can be expected to be somewhat better if the AFR is kept identical in both cycles (i.e. the comparison takes place at the same load in both cycles).

In short, although the boost pressure in the **2V-TC** Atkinson cycle implementation is more than five times higher at virtually the same IMEP, only a minor improvement of the TCE can be detected. For this reason, the implementation of the Atkinson cycle by means of a significant delay of the suction and a strong enhancement of the charge pressure applied to a classic Seiliger cycle does not represent a suitable solution. Therefore, a new approach is needed to implement a **real Atkinson cycle**.

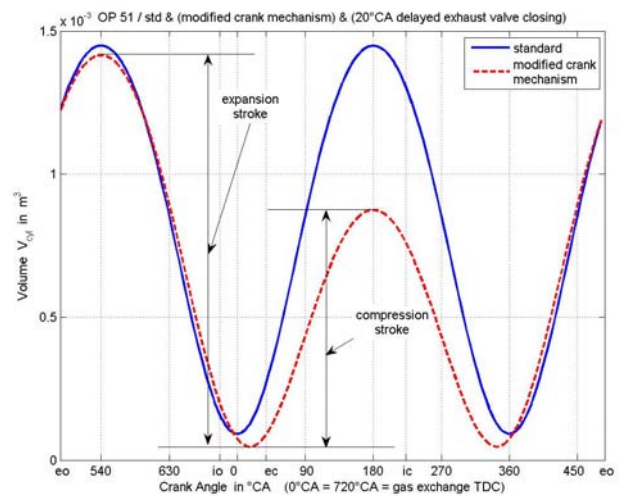
Figure 15a. Relative Piston Displacement – CA Diagram for an aspirated engine [4]. Intake and compression strokes of modified crankshaft drive are shorter than expansion and exhaust strokes
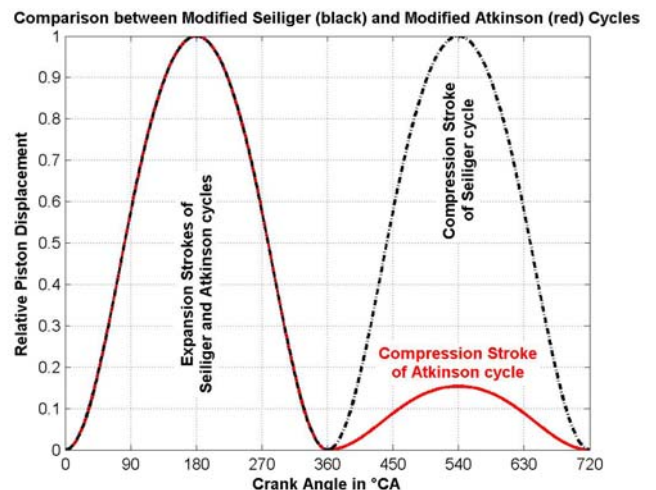

Figure 15b. Relative Piston Displacement – CA Diagram for a very high pressure supercharged engine [8]. The intake and compression strokes are very much shorter than expansion and exhaust strokes

2. ATKINSON CYCLE IMPLEMENTATIONS TO ICE WITH ASYMMETRICAL CRANKSHAFT DRIVE = STRICT ATKINSON CYCLE IMPLEMENTATION

The goal of the present investigations is to attempt to propose better implementations of the Atkinson cycle in accordance with the previously presented restrictions.

In order to realize a strict Atkinson cycle - i.e. shortened compression and extended expansion - a special crankshaft drive is proposed, which permits geometrically different strokes for compression and expansion (see Fig. 15a for aspirated engines [4], respectively 15b for supercharged engines [8]). The design of this crankshaft drive is not the subject of this investigation and is therefore not described here. Its mechanical efficiency is estimated to be more than 96%. Many crank mechanisms with asymmetrical strokes are already patented in several variants, or have reached the stage of application for a patent.

2.1 Analysis of Atkinson cycle implementation for aspirated ICE

The aim here is merely to estimate the potential for increasing the TCE and IFCE if the crankshaft drive from Figure 15a is used. In other words, this implementation of the Atkinson cycle, labelled further on as the third variant or 3V (see [4] for more details), investigates the extent to which losses caused by the suction and partial expulsion of the fresh charge reduce the IFCE.
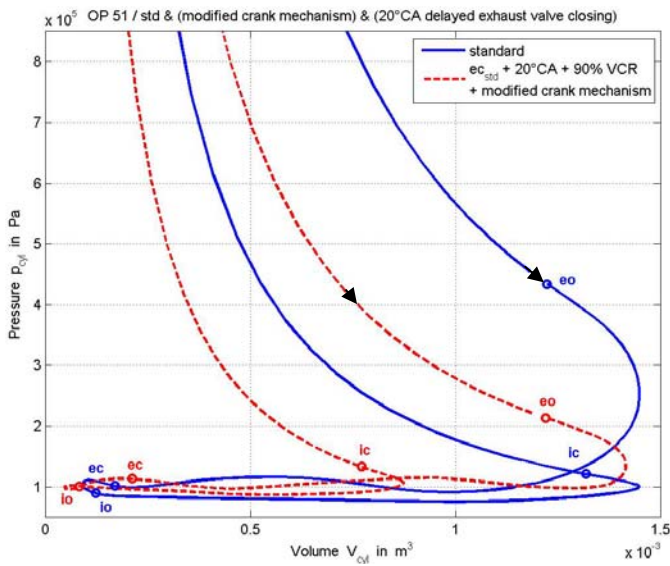

Figure 16. Pressure – Volume Diagram [4]

As before, a comparison is made with the Seiliger cycle from Figures 2, 4 and 5 (i.e. standard variant or SV). As the angle positions of the top dead centre are slightly shifted compared to the SV in this modified crankshaft drive, the closing angle of the exhaust valve in the 3V is also 20°CA delayed in order to avoid causing large counter pressure during the valve overlap time.

The p,V diagram is shown in Figure 16, in which both the different compression and expansion strokes and also the

increased compression ratio can clearly be recognized for the modified crankshaft drive. An analysis of the T,s and of the (much pronounced) T,s* diagrams from Figure 17 reveals that the TCE is higher in the 3V than in the SV. The only factor which could have contributed to this is the elimination of the back and forth streaming through the intake valve, since no other changes or parameter optimizations were made compared to the Atkinson cycle implementation presented in Figures 2, 4 and 5. Note that a) the areas beneath the lower curves up to the temperature of 0 K represent the "lost" specific heat q_{ab} (here really as a result of the gas exhaust from cylinder between **eo** and **ec**, see Fig. 17) and b) in the case of reversible processes on the cycle (as in this case) the TCE is equivalent to the IFCE of the cycle.
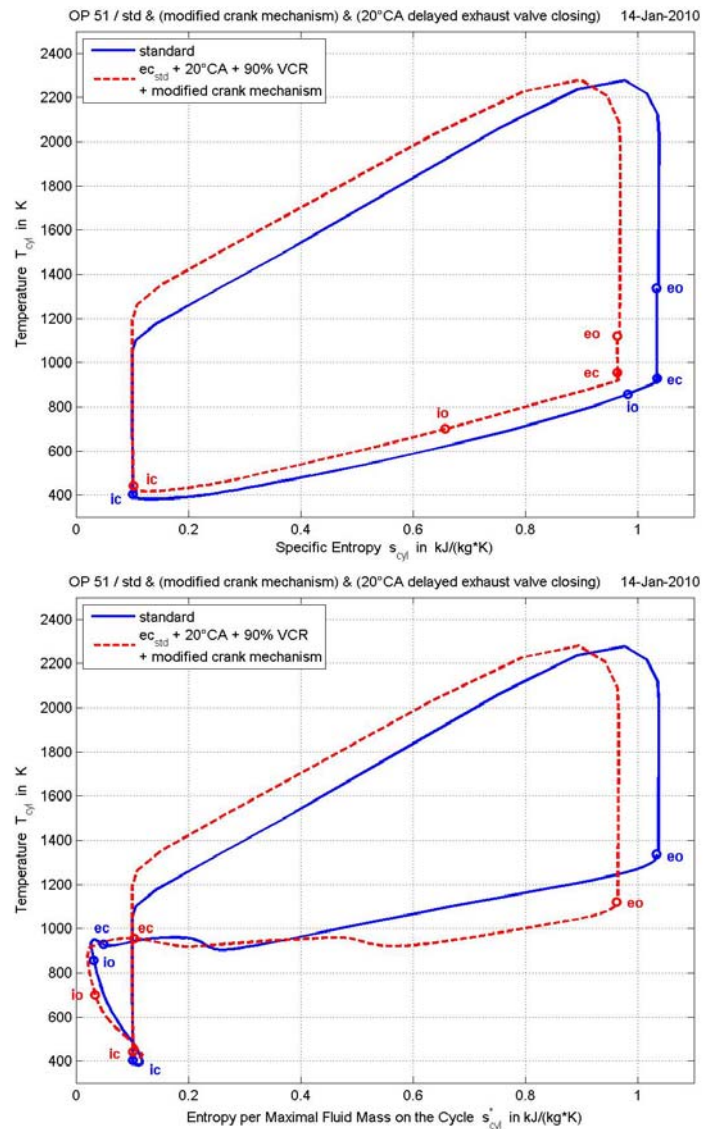

Figure 17. Temperature – Specific Entropy (T,s) [4] and Temperature – Entropy per Max. Fluid Mass diagrams (T,s*)

The curve of the cylinder mass from Figure 18 confirms that the entire aspirated gas mass remains in the cylinder for combustion. Although the compression stroke is much shorter

than in **2V** and the intake valve is opened for a shorter time, the mass sucked in **3V** is roughly 6% greater than in **2V**.

The analysis of the curves in Figure 19 shows the same situation as in Figure 2, where more piston work is needed in **2V** and **3V** for emptying the cylinder in comparison to **SV** (see **A** areas in both figures). After the intake valve has closed and the compression has started, the IFCE drops again sharply in the case of **3V** as a result of the increased VCR, but less sharply than in the case of **2V** (compare **C** areas in both figures) because of the elimination of back streaming through the intake valve (see **B** area in Figure 2 for **2V**). A 15% increase of IFCE is therefore achieved after compression and expansion in **3V**, compared to **SV** and **2V**.
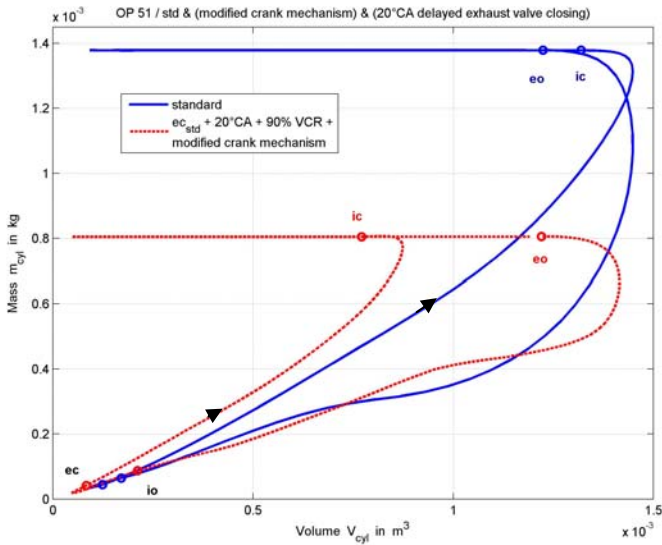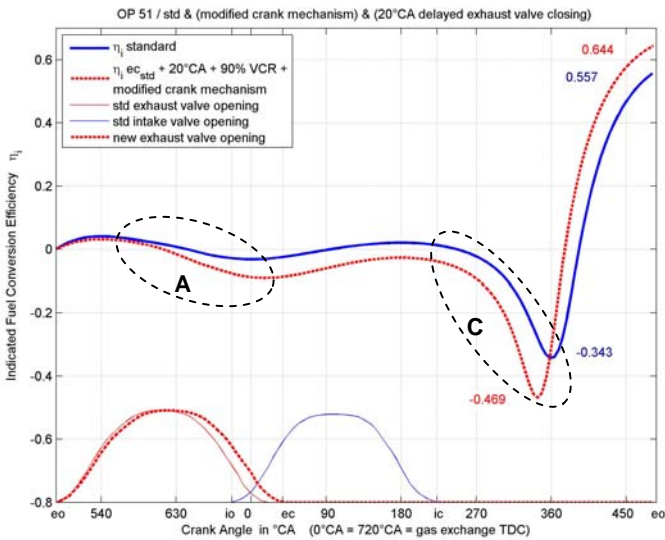

Figure 18. Fluid Mass – Volume Diagram [4]

Figure 19. IFCE – Crank Angle Diagram [4]

2.2 Analysis of Atkinson cycle implementation TO ICE with very high charge pressure

2.2.1 *Ideal V,p,T Model of Seiliger and Atkinson Cycles*

In the case of supercharged ICE, the number of parameters which influence the TCE becomes much higher. As a consequence, the effort to achieve combinations of parameters which maximize the TCE of the **real** ICE cycle becomes much more difficult. For these reasons, **ideal models of the V,p,T-Seiliger and -Atkinson cycles** are developed for this purpose.

Modelling by means of V,p,T-Seiliger and -Atkinson cycles (see Fig. 1) has the advantage of allowing users to generate ideal engine cycles which model the real ICE cycles more accurately than the classic ideal V- and V,p-cycles by observing their mechanical (pressure) and thermal limits. A simple V-cycle (Otto cycle), where the heat is released only in an isochoric manner (constant volume), generates unrealistically high maximum pressure and temperature levels on the cycle. The attempt to limit the maximum pressure level leads to the classic V,p-cycle [1], [2], where the heat is released in an isochoric and isobaric (constant pressure) manner. The V,p-cycles (i.e. classic Seiliger cycles) leads, for example, to very high temperature levels in the case of fully loaded supercharged engines, which are completely unrealistic.

In this recently introduced ideal V,p,T-cycle the heat is partially released isochorically on $2 - 3v$, isobarically on $3v - 3p$ and isothermally on $3p - 3$ change of states (see Figures 1 and 20). The amounts of heat released are determined to satisfy the targets for maximum pressure p_{max} and temperature T_{max} on the cycle. The compression $1 - 2$, expansion $3 - 4$, emptying $4 - 5$ and $5 - 6$ as well as the filling $6 - 7$ and $7 - 1$ are adiabatic. In this ideal cycle no other losses are taken into consideration (i.e. all the processes in this cycle are reversible). Pressure and temperature remain constant during expansion $5 - 6$ and filling $7 - 1$. The theoretical background of the V,p,T-cycle is presented in the Appendix.

Simulations with BOOST (**real models** of ICE cycles) are used afterwards as a reference in order to evaluate the accuracy and the prediction accuracy of these ideal models on the TCE. The purpose of the BOOST simulations is not to obtain a perfect overlapping of the curves in the following diagrams, but rather to demonstrate that the proposed V,p,T-model is able to produce good results and accurate predictions of the influence that many parameters have on the TCE without a major computing effort. The heat release function of the BOOST model from Figure 6 was not optimized for a better overlapping of cycles. This function is modelled with the help of a simple Vibe function. As a consequence, the pressure peak of the Boost simulation (see Fig. 21) exceeds the proposed maximum pressure p_{max} and it behaves differently depending on temperature and the variation of cylinder volume (see Fig. 23). Note that the increase of the gas mass by injection of the fuel during the high pressure processes was not taken into consideration in the ideal V,p,T model (see Fig. 25).

2.2.2 *Comparison of Seiliger and Atkinson Cycles at Full Load using the Ideal V,p,T - Model*

A V,p,T-Seiliger cycle and a V,p,T-Atkinson cycle are simulated and compared (see Fig. 20, 22 and 24). To facilitate this comparison, the following parameters are kept identical in

both cycles: expansion ratio ε_e, specific released heat q_{zu}, air-fuel-ratio λ, isentropic exponent κ (constant), maximal pressure p_{max} and temperature T_{max} on the cycle and charge temperature, i.e. of the fresh air after compressor and cooler, T1 = TC (see parameter boxes in the figure):
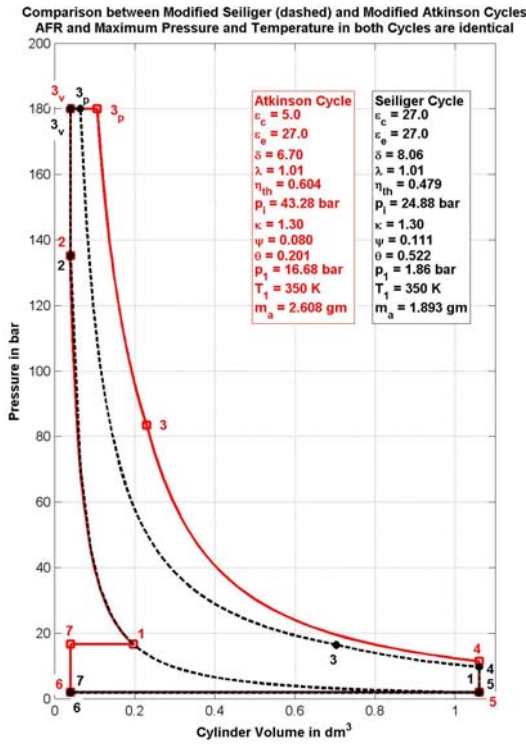

Figure 20. Pressure – Volume Diagram of V,p,T–Seiliger and –Atkinson Cycles
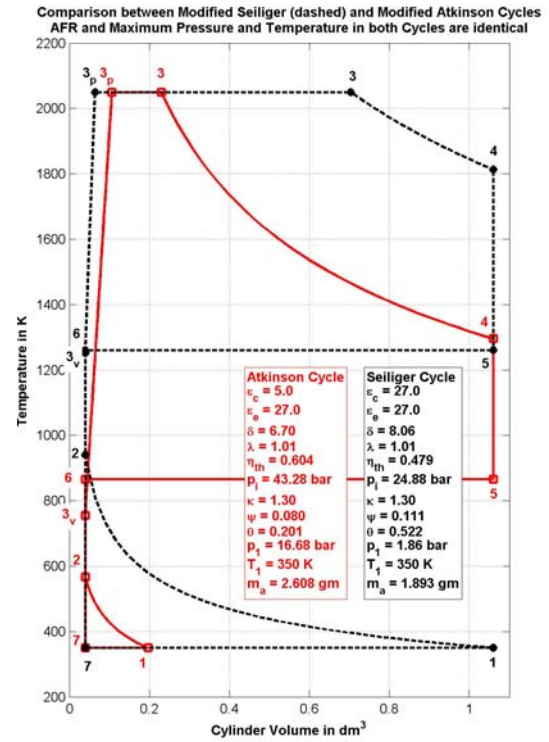

Figure 22. Temperature–Volume Diagram of V,p,T– Seiliger and –Atkinson Cycles
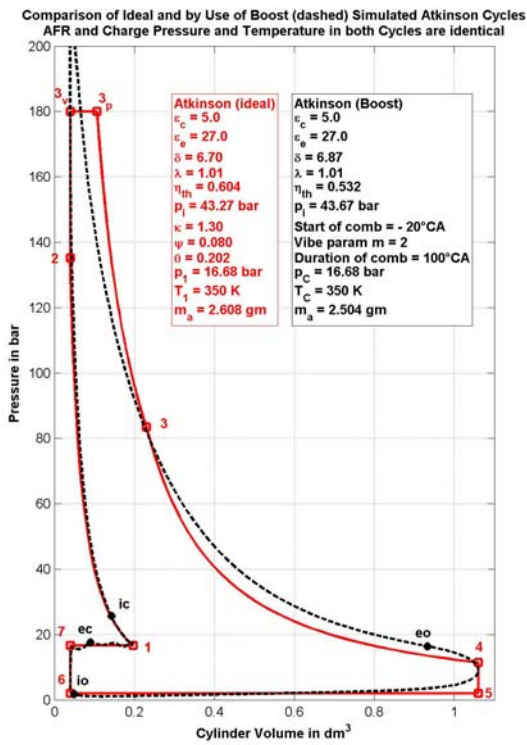

Figure 21. Pressure – Volume Diagram of V,p,T– and BOOST Model for the Atkinson Cycle
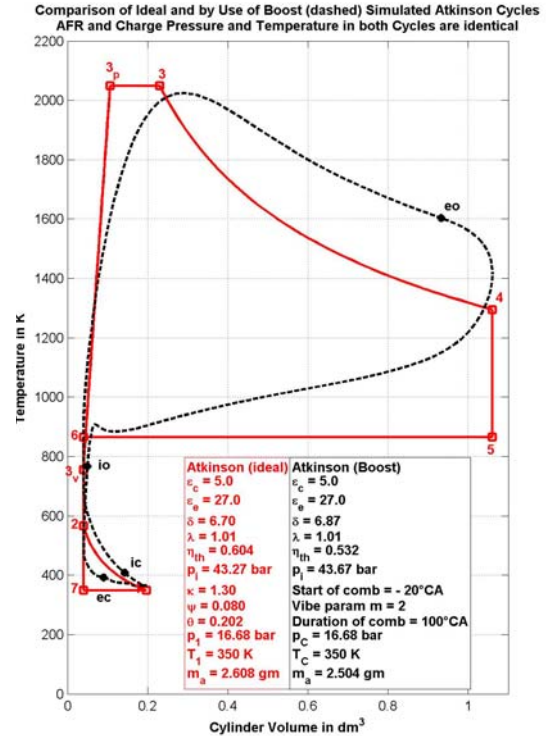

Figure 23. Temperature – Volume Diagram of V,p,T–and BOOST Model for the Atkinson Cycle

In the Seiliger cycle the expansion and compression ratios are identical. In the Atkinson cycle, a very low compression ratio and a very high boost pressure $p_1 = p_C$ are chosen, meaning that state 1 of the Atkinson cycle is overlaid on the compression curve 1-2 of the Seiliger cycle (see Figure 20). In this way, the full potential of the turbo charging can be used without exceeding the maximum pressure (in this case $p_{max} = 180$ bar) and temperature (in this case $T_{max} = 2050$ K) on the cycle.

The charge pressure p_1 in the Atkinson cycle from Figures 20 and 21 is unusually high. Such turbo charging systems are not typical at this time for ICE because the maximum pressure p_{max} on the cycle severely limits the level of charge pressure in classic (i.e. Seiliger cycle) applications. For this reason, the current classic, highly supercharged, diesel engines must either decrease the VCR or the aspirated air mass sharply ([1], [2], [7]) in order to avoid exceeding the maximum pressure during the cycle. These restrictive measures substantially limit the TCE of these cycles.

For these reasons, this paper has searched for ways to make better use of the enthalpy of the exhaust gases. In the case of stoichiometric AFR, this enthalpy is more than enough to provide the compression of the fresh charge up to the very high pressure p_1 of the V,p,T-Atkinson cycle from Figure 20. On the other hand, the temperature of the fresh charge T_1 must be kept low by means of intensive cooling after each turbo compressor stages. The high level of p_1, the low level of T_1 and the reduced piston work for compression significantly increase the TCE η_{th} on this cycle.

In addition, the piston work for gas exchange processes becomes highly positive, i.e. this piston work is supplied for the Atkinson cycle instead of being consumed as in the case of Seiliger cycle (see Fig. 20).

As a result, the TCE of the Atkinson cycle is more than 25% greater than that of the Seiliger cycle. At the same time, the indicated mean pressure (p_i or IMEP) of the Atkinson cycle exceeds that of the Seiliger cycle by more than 70%, while meeting the same mechanical and thermal limits in both cycles (see Fig. 20 and 22).

How is that possible? The states depicted in Figure 22 show that the temperature at the end of compression T_2 in the Atkinson cycle is much lower because of the lower VCR of this cycle. The isochoric-released heat fractions ψ (needed to achieve p_{max}) in the Atkinson and Seiliger cycles are very much equal. The isothermal released heat fraction θ during the Atkinson cycle, however, becomes much lower than that of the Seiliger cycle (see positions of states 3p and 3 for the Seiliger cycle in Fig. 20 and 22). A bigger isothermal-released (compared with isochoric and isobaric) heat fraction leads to lower TCE (see the curves of these influences in Figures 28 and 29). These facts explain for the main part the better TCE of the Atkinson cycle.

The diagrams of Figures 24 and 25 are presented for a better understanding of the filling and emptying processes. Along the horizontal curves of Figures 24 and 25 the cylinder is closed, the filling process takes place between the states $6 - 7 - 1$, and the empting process takes place between the states $4 - 5 - 6$. As the temperature at the end of the filling is kept at the same level in both cycles, the sucked fresh charge mass in the Atkinson

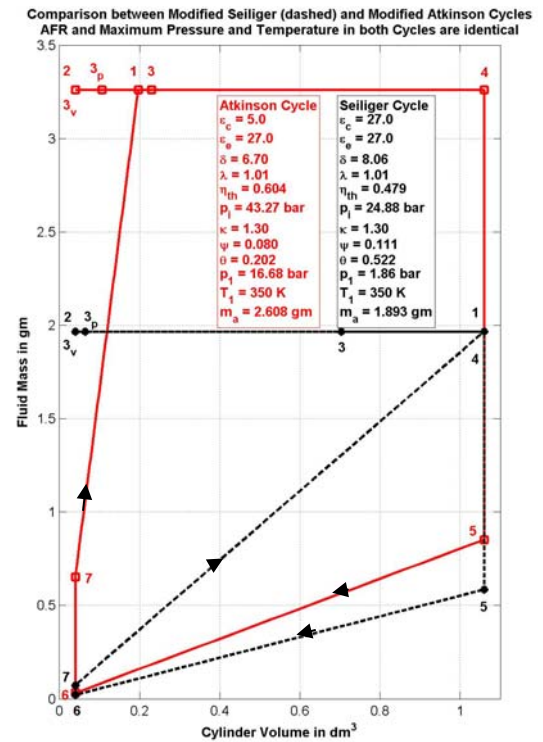cycle is greater than that of the Seiliger cycle. This explains the bigger IMEP (or p_i) of the Atkinson cycle.

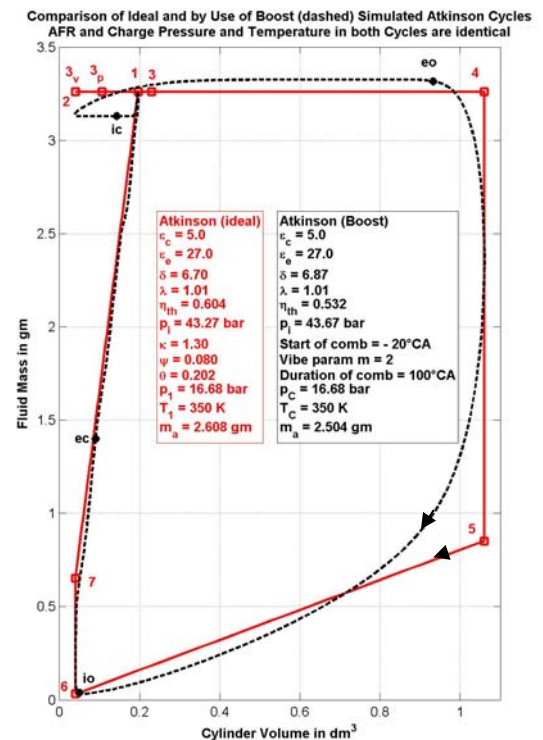**Figure 24.** Fluid Mass – Volume Diagram of V,p,T– Seiliger and –Atkinson Cycles [8]

Figure 25. Fluid Mass – Volume Diagrams of V,p,T– and BOOST Model for Atkinson Cycle [8]

2.2.3 _Analysis of Atkinson Cycle Implementations over all EOP using the Ideal V,p,T - Model_

The implementation of the Atkinson cycle by means of the asymmetrical crank drive has the disadvantage that at part loads - because of the very extensive expansion - the cycle stops being feasible, i.e. the pressure at the end of expansion becomes lower than the ambient pressure (see Appendix, Requirements for cycle realization). For this reason, the crank drive should also enable the variation of the VCR, as presented in Figure 26.
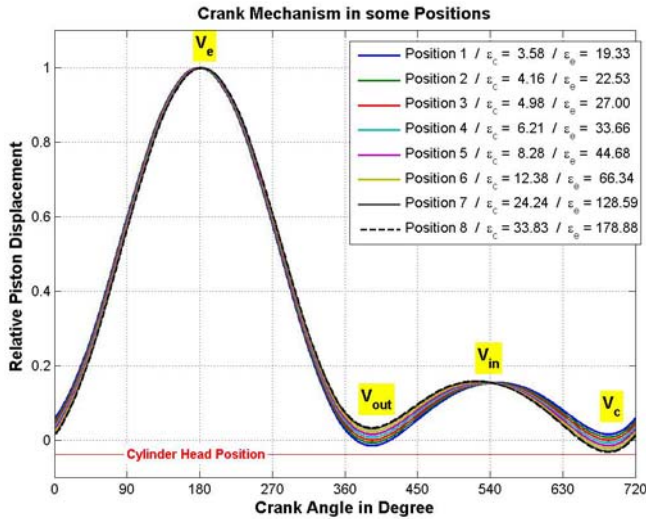

Figure 26. Relative Piston Displacement of an Asymmetrical Crank Mechanism with variable VCR

Using such a crank mechanism, it is possible to realize Atkinson cycles for part loads even with stoichiometric AFR and without throttling. For example, the pressure-volume, temperature-volume, fresh charge mass-volume and temperature-specific entropy diagrams for Position 1 of the crank mechanism (see Figure 26) at full and many part loads are presented in Figure 27. The best TCE is reached for a boost pressure of ca. 10 bar.

For this position of the crank mechanism and for the stoichiometric AFR, the limits for the boost pressure are between 2 and 34 bar. For the other positions of the crank mechanism, these limits are different. These boost pressure limits are set by requirements 1 to 5 for cycle realization and the formula for the ideal V,p,T model (see Appendix).

The states 1 to 7 marked on the magenta cycle in the four diagrams of Figure 27 correspond to an 18 bar boost pressure. The red cycle corresponds to a 10 bar boost pressure and has the best TCE for this crank mechanism position. The T,s diagram from **B**, and more evidently the T,s* diagrams from **D**, confirm that this cycle has the highest TCE.

Figure 28 depicts the correlations between TCE, IMEP, boost pressure and crank mechanism positions for the stoichiometric AFR. The arrows show this correlation for position 1 of the crank mechanism where the TCE reaches its maximum. The boost pressure was not limited in these simulations to the current usual maximum values. Whether or not such high boost pressure values are at present achievable is not the subject of this investigation and therefore not discussed here.
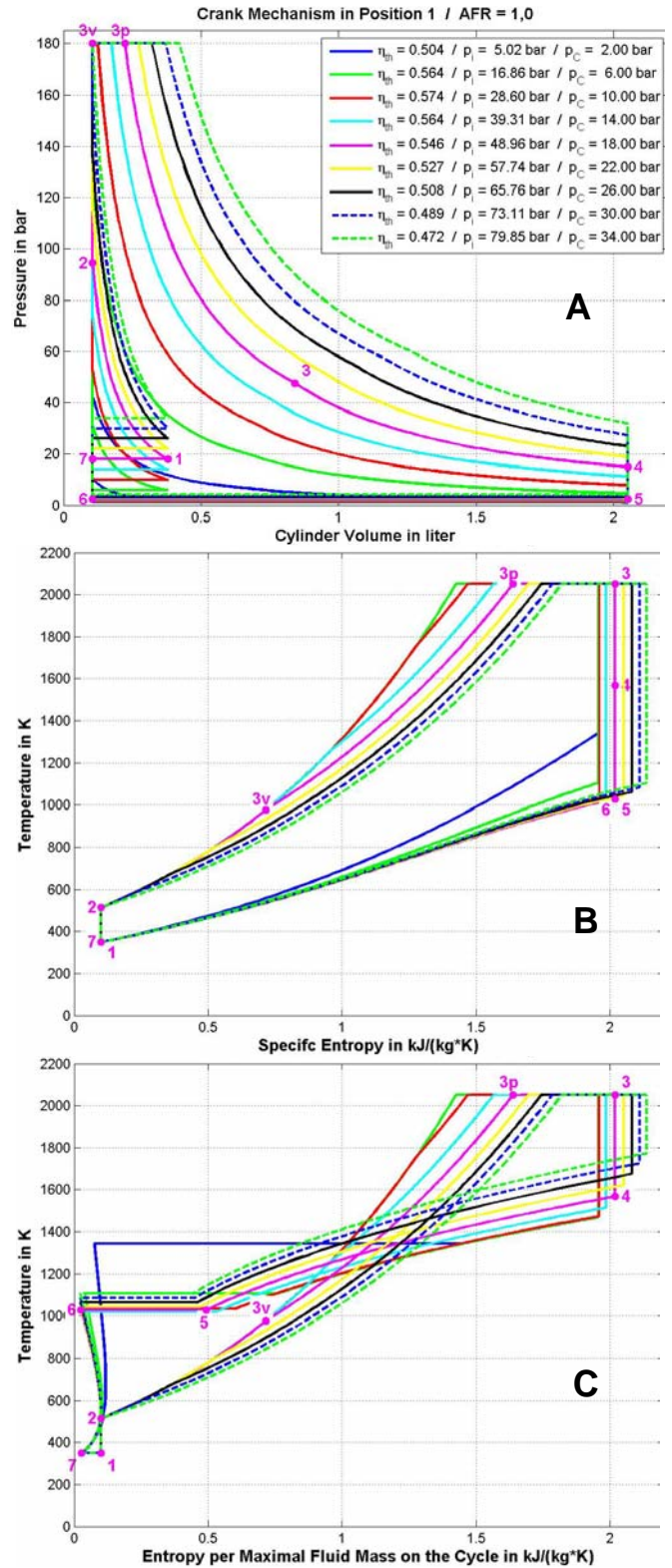

Figure 27. Simulated Ideal V,p,T Atkinson Cycles for the Crank Mechanism in Position 1 (see Fig. 26) at Full and many Part Loads with Stoichiometric AFR. **A** represent Pressure-Volume (p,V), **B** Temperature-Specific Entropy (T,s) and **C** Temperature-Entropy per Max. Fluid Mass diagrams (T,s*)
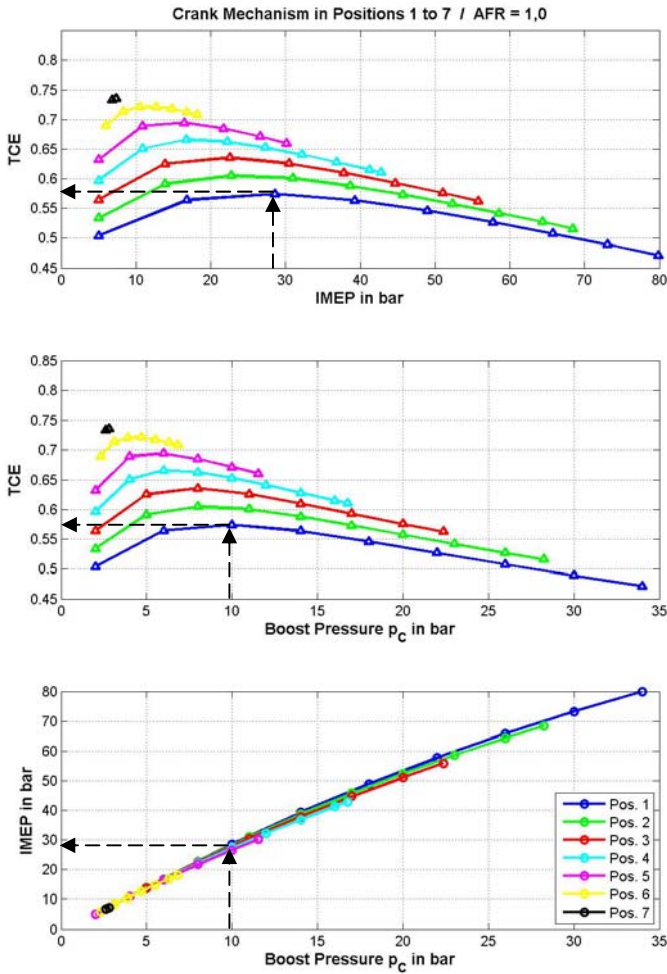
Figure 28. Correlation between TCE, IMEP, Boost Pressure and Crank Mechanism Positions at Full and many Part Loads with Stoichiometric AFR
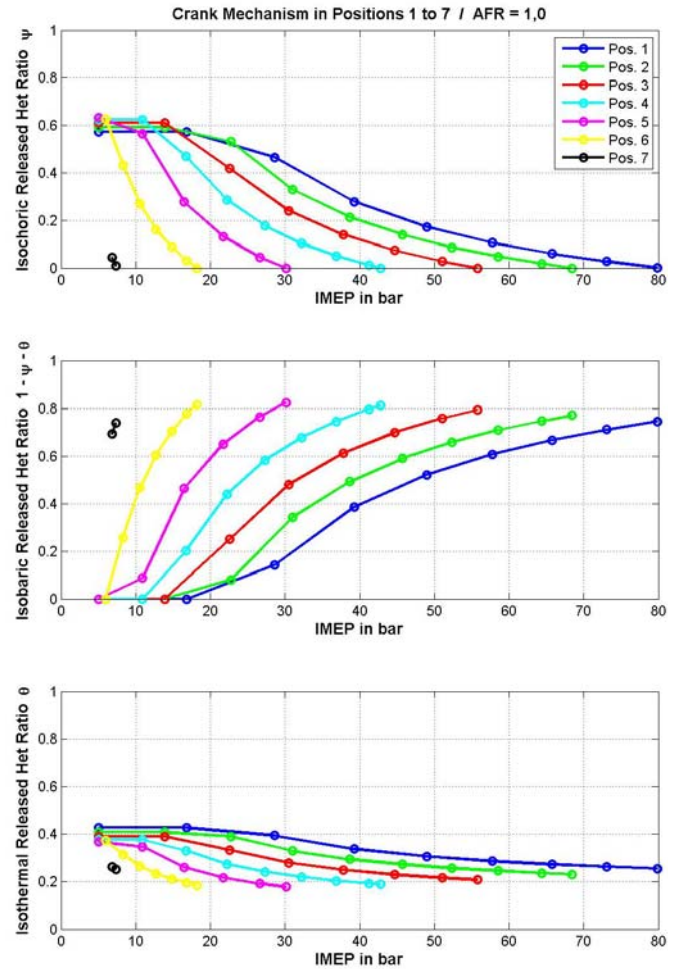

Figure 29. Heat Release Fractions - IMEP Diagrams for many Crank Mechanism Positions (see Fig. 26) at Full and many Part Loads with Stoichiometric AFR

Figure 29 presents the corresponding combinations of the heat release fractions for achieving the performances from Figure 28. The isochoric fractions of the released heat are highest (as expected for reaching the maximum of TCE) for the lowest part load in all positions of the crank mechanism, with the exception of 7. This level of the isochoric fractions cannot be maintained in all other EOPs because of the p_{max} restriction.

An imaginary curve, which tops all the TCE-IMEP curves of the Figure 28 diagram, shows, for example, that the TCE remains much higher than 60% in the case of IMEP values ranging between 5 and 40 bar for stoichiometric AFR, when the crank mechanism position is changing continuously from 7 to 4 and the boost pressure changes accordingly between 2 and 15 bar.

The increase in AFR from 1 (i.e. stoichiometric) to 2, for example, should theoretically improve the TCE values because the load decreases. That behaviour is confirmed in Figures 30 and 31. As less heat is available on the cycle when AFR = 1.5 or 2, this heat may only be released isochorically and isobarically without exceeding the limits p_{max} and T_{max}. As a result, the TCE values are higher for this lean mixture than in the stoichiometric case (see Fig. 30 and 31).

The question here is whether the exhaust gas energy for turbo charging is sufficient for achieving the required high boost pressure. Figures 32 and 33 depict the pressure and temperature of exhaust gases before turbine and the relative energy balance on the turbocharger for stoichiometric and AFR = 1.5. The values of the isentropic efficiency of compressor and turbine used in these simulations are η_{sc} = 0.75 and η_{sT} = 0.65.

The relative energy for turbo charging (**RE4T**) is defined as the quotient of a) the difference of the works of turbine and compressor and b) the piston work on the cycle (all these works are considered positive here). Its variations are depicted in the bottom diagrams of Figures 32 and 33, where the positive values show that the requirement for turbo charging (see Appendix, 5th requirement) is met. The cycles with positive values of RE4T are marked by triangles in Figures 28, 30 and 31. The other cycles (marked by circles) cannot be realized without the use of a supplementary mechanical compressor.

We can conclude that, for the stoichiometric AFR, the exhaust gases have enough energy (i.e. enthalpy) for realizing the necessary boost pressure in all EOP from Figures 28, 29 and 32. In the case of AFR = 1.5, the enthalpy of the exhaust

gases is sufficient only for a few points at the lowest part load (see **A** area in Fig. 33).
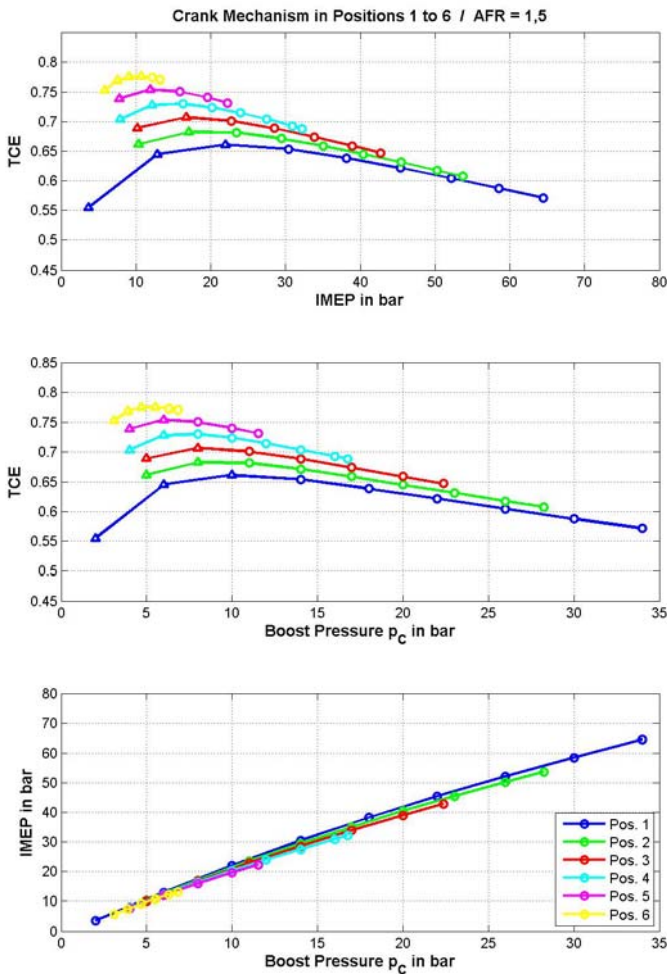

Figure 30. Correlation between TCE, IMEP, Boost Pressure and Crank Mechanism Positions at Full and many Part Loads with AFR = 1.5

CONCLUSION

The TCE gain of the Atkinson cycle implementation on **aspirated engines** - like Toyota has done in Prius II - by means of delaying the intake valve closing and by increasing the VCR is modest and largely dependent on the fine-tuning of all control parameters (valve timing etc.). In addition, the specific power of the engine is low because of the lower retained mass of fresh charge in the cylinder before compression. For these reasons, this implementation of the Atkinson cycle is only suitable for hybrid vehicles, where the engine - because it is not directly linked mechanically to the wheels - works only in its best operating range and in combination with an electric motor.

The simulation results for the Atkinson cycle implementation on **supercharged engines**, where the intake valve closing is 60°CA delayed, shows that TCE and IMEP are 6% less than in the standard version although the boost pressure

is 40% higher. In addition, the implementation of the Atkinson cycle is investigated by means of an important delaying of the suction and strong enhancement of the charge pressure. Although the boost pressure in this Atkinson cycle implementation is more than five times greater at virtually the same IMEP, there is only a minor improvement in the TCE.
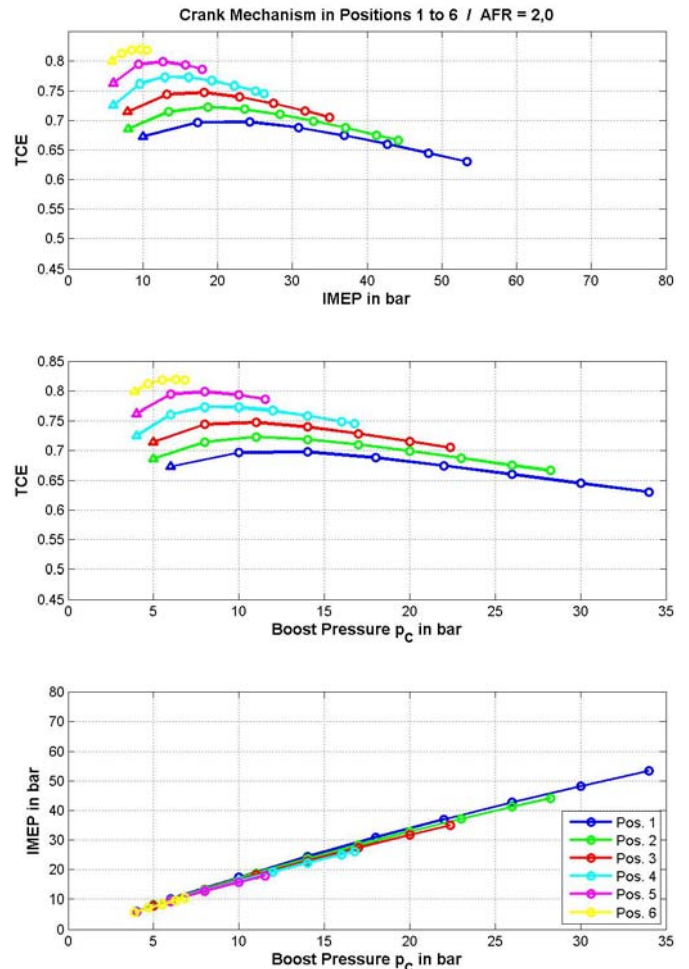
Figure 31. Correlation between TCE, IMEP, Boost Pressure and Crank Mechanism Positions at Full and many Part Loads with AFR = 2

For these reasons, a new approach is needed to implement a **real Atkinson cycle** on aspirated and supercharged engines. In order to realize a strict Atkinson cycle - i.e. shortened compression and extended expansion - a special crankshaft drive is proposed, which permits geometrically different strokes for compression and expansion.

An analysis of the simulation results for the implementation of Atkinson cycles on **aspirated engines with an asymmetrical crank drive** shows that a 15% increase in IFCE can be achieved.

In the case of **supercharged engines**, the number of parameters which influence the TCE becomes much higher. As a consequence, the effort to achieve combinations of parameters which maximize the TCE of **real** ICE cycle

becomes much more difficult. For these reasons, **ideal models of the V,p,T-Seiliger and -Atkinson cycles** are developed for this purpose (see Appendix).

Figure 32. p_T-, T_T- and RE4T - Boost Pressure Diagram for seven Crank Mechanism Positions at Full and many Part Loads with stoichiometric AFR

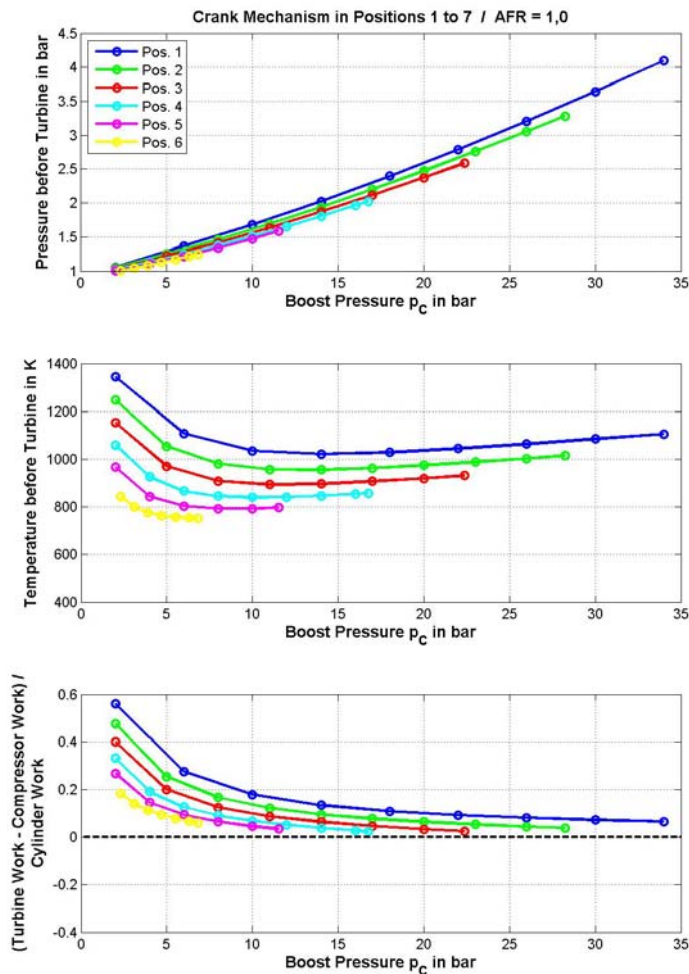The TCE of the Atkinson cycle implemented in **supercharged engines with asymmetrical crank drive** is more than 25% better and the IMEP exceeds that of the Seiliger cycle by more than 70%, while meeting the same mechanical and thermal limits in both cycles.

The implementation of the Atkinson cycle by means of the asymmetrical crank drive has the disadvantage that at part loads - because of the very extensive expansion - the cycle stops being feasible, i.e. the pressure at the end of expansion becomes lower than the ambient pressure (see Appendix, Requirements for cycle realization). For this reason, an asymmetrical crank mechanism is required which also enables the variation of the VCR.

By using such a crank mechanism, it is possible to realize Atkinson cycles for part loads even with stoichiometric AFR and without throttling.
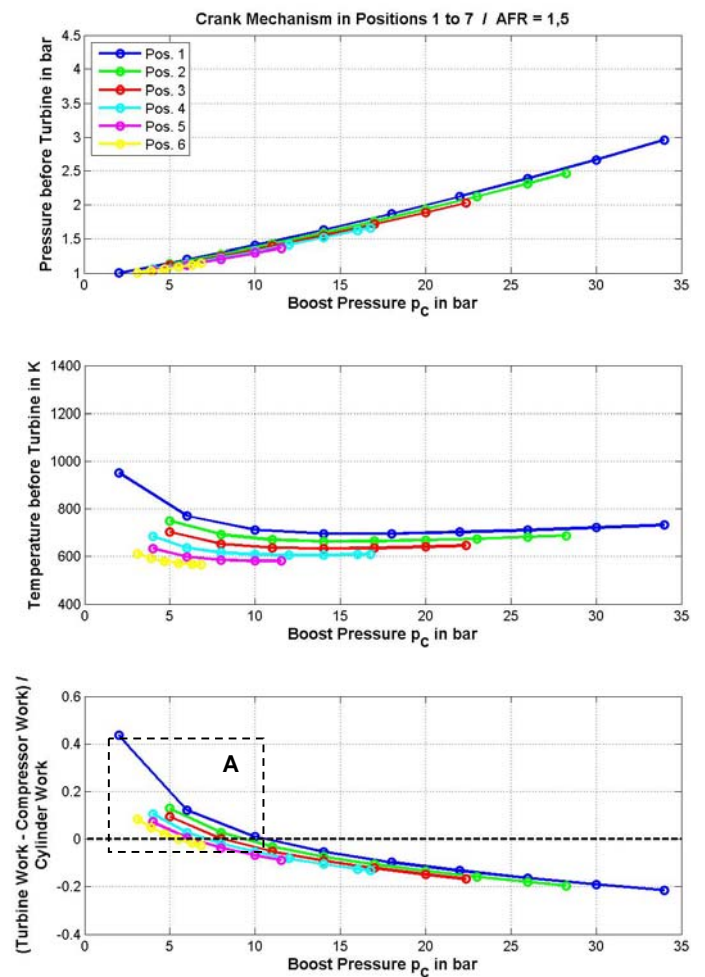
Figure 33. p_T-, T_T- and RE4T - Boost Pressure Diagram for six Crank Mechanism Positions at Full and many Part Loads with AFR = 1.5

REFERENCES

1. Heywood, JB, Internal Combustion Engine Fundamentals, MacGraw-Hill Book Company, 1988
2. Pischinger, A, Kraβnig, G, Taucar, G, & Sams, Th,, Thermodynamic of Internal Combustion Engines (German), Springer-Verlag, Wien New York, 1989
3. Toyota Hybrid System (THS) II, Toyota Motor Corporation, Public Affairs Division, Japan, 2003
4. Gheorghiu, V, Enhancement Potential of the Thermal Efficiency of ICE Cycles Especially for Use into Hybrid Vehicle, HEFAT 2007, 5th International Conference on Heat Transfer, Fluid Mechanics and Thermodynamics, Paper number: GV1, July 2007, Sun City, South Africa
5. Gheorghiu, V, Higher Accuracy through Combining of quasi-3D (instead of 1D) with true-3D Manifold Flow Models during the Simulation of ICE Gas Exchange Processes, 2001-01-1913, SAE Congress, Orlando, Florida, USA, 2001

6. Gheorghiu, V, Simulation Results of Compressible Unsteady Flows Through ICE Manifolds, F2004F427, FISITA Congress, Barcelona, Spain, 2004
7. Schutting, E, Neureiter, A, Fuchs, Ch., Schwarzenberger, T, Klell, M, Eichlseder, H, Kammerdiener, T, Miller- and Atkinson-Cycle for Supercharged Diesel Engines, MTZ 06 / 2007 (German)
8. Gheorghiu, V, CO2-Emission Reduction by means of Enhanced Thermal Conversion Efficiency of ICE Cycles, ICE200 09ICE-0130 / SAE 2009-24-0081, ICE, Neapel, Italy, 2009

DEFINITIONS

Symbol	Meaning	Units
$\delta = \dfrac{q_{zu}}{c^\circ_v \cdot T_1}$	relative released heat as measure of engine load	-
$q_{zu.v}$	isochoric part of q_{zu}	$\dfrac{J}{kg}$
$\psi = \dfrac{q_{zu.v}}{q_{zu}}$	isochoric released heat fraction	-
$q_{zu.t}$	isothermal part of q_{zu}	$\dfrac{J}{kg}$
$\theta = \dfrac{q_{zu.t}}{q_{zu}}$	isothermal released heat fraction	-
$1 - \psi - \theta$	isobaric released heat fraction	-
$\phi = \dfrac{p_T}{p_C}$	turbine to compressor pressure ratio	-
$\eta_{th} = \dfrac{-w_{cycle}}{q_{zu}}$	thermal conversion efficiency	-
w_{cycle}	specific work on the all cycle	$\dfrac{J}{kg}$
$p_i = IMEP$	indicated mean pressure	bar
η_{sC}, η_{sT}	isentropic efficiency of compressor and turbine	-
W_{TTu}	turbine work between p_T and p_u	J
W_{CuC}	compressor work between p_u and p_C	J
io, ic	intake valve open & close locations	
eo, ec	exhaust valve open & close locations	
u	ambient state index	

ABBREVIATIONS

AFR	Air-Fuel Ratio
CA	Crank Angle
EOP	Engine Operating Point
ICE	Internal Combustion Engine
IFCE	Indicated Fuel Conversion Efficiency
IMEP	Indicated Mean Pressure
RE4T	Relative Energy for Turbo charging
SI	Spark Ignition Engine
TCE	Thermal Conversion Efficiency
VCR	Volumetric Compression Ratio

Symbol	Meaning	Units
$\varepsilon_c = \dfrac{V_1}{V_2} = \dfrac{V_{in}}{V_c}$	volumetric compression ration	-
$\varepsilon_e = \dfrac{V_5}{V_2} = \dfrac{V_e}{V_c}$	volumetric expansion ratio	-
$V_{in} = V_1$	cylinder volume at end of suction	m^3
$V_c = V_2 = V_{3v}$	cylinder volume at end of compression	m^3
$V_e = V_4 = V_5$	cylinder volume at end of expansion	m^3
$V_{out} = V_6 = V_7$	cylinder volume at end of emptying	m^3
$V_{max} = V_4 = V_5$	maximal cylinder volume	m^3
$p_{max} = p_{3v} = p_{3p}$	maximal pressure on cycle	Pa
$p_{max.0}$	desired value of p_{max}	Pa
$p_{max.\psi 1}$	p_{max} for 100% isochoric heat release	Pa
$p_C = p_1$	charge pressure after cooler	Pa
$p_{C.0}$	desired value of p_C	Pa
p_T	pressure before turbine	Pa
$T_C = T_1$	charge temperature after cooler	K
$T_{C.0}$	desired value of T_C	
$T_{max} = T_{3p} = T_3$	maximal temperature on cycle	K
$T_{max.\psi 1}$	T_{max} for 100% isochoric heat release	K
m_a	fresh charge mass per cycle	kg
$m_1 = m_a \cdot \varepsilon_a$	cylinder gas mass in state 1	kg
m_f	fuel mass per cycle	kg
$\kappa = \dfrac{c^\circ_p}{c^\circ_v}$	isentropic exponent	-
c°_p, c°_v	isobaric & isochoric specific heat capacity	$\dfrac{J}{kg \cdot K}$
λ	air-fuel ratio (AFR)	-
L_{st}	stoichiometric air requirement ratio	$\dfrac{kg \cdot air}{kg \cdot fuel}$
H_u	fuel lower heating value	$\dfrac{J}{kg}$
$q_{zu} = \dfrac{\eta_b \cdot m_f \cdot H_u}{m_1}$	released heat per unit fluid mass	$\dfrac{J}{kg}$
η_b	released fuel energy completeness	-

SV	Standard Variant for Aspirated Engine
2V	Second Variant for Aspirated Engine
3V	Third Variant for Aspirated Engine
1V-TC	First Variant for Turbo Charged Engine
2V-TC	Second Variant for Turbo Charged Engine
io	Intake Valve Open
ic	Intake Valve Close
eo	Exhaust Valve Open
ec	Exhaust Valve Close

APPENDIX / FORMULA

Formula for the ideal V,p,T-model

$$\delta = \frac{H_u \cdot \eta_b}{\lambda \cdot L_{st} \cdot c^\circ_v \cdot T_C \cdot \varepsilon_a}$$

$$\varepsilon_a = \frac{\dfrac{V_{in}}{V_{out}}}{\dfrac{V_{in}}{V_{out}} - 1}$$

$$p_C = \min\left(p_{C.0}, \frac{p_{max.0}}{\varepsilon_c^{\,\kappa}}\right)$$

$$T_{max.\psi1} = T_C \cdot \left(\varepsilon_c^{\,\kappa-1} + \delta\right)$$

$$T_{max} = \min\left(T_{max.0}, T_{max.\psi1}\right)$$

$$p_{max.\psi1} = p_C \cdot \left(\varepsilon_c^{\,\kappa} + \delta \cdot \varepsilon_c\right)$$

$$\psi_{Tmax} = \frac{1}{\delta} \cdot \left(\frac{T_{max.0}}{T_C} - \varepsilon_c^{\,\kappa-1}\right)$$

$$\psi_{pmax} = \frac{1}{\varepsilon_c \cdot \delta} \cdot \left(\frac{p_{max.0}}{p_C} - \varepsilon_c^{\,\kappa}\right)$$

$$\psi = \min\left(\psi_{Tmax}, \psi_{pmax}, 1\right)$$

$$p_{max} = p_C \cdot \varepsilon_c \cdot \left(\varepsilon_c^{\,\kappa-1} + \psi \cdot \delta\right)$$

$$\theta = 1 - \psi - \frac{\kappa}{\delta} \cdot \left(\frac{T_{max}}{T_C} - \varepsilon_c^{\,\kappa-1} - \psi \cdot \delta\right)$$

$$\theta = \max(\theta, 0)$$

$$a = \frac{\varepsilon_c^{\,\kappa-1}}{\delta} + \psi + \frac{1 - \psi - \theta}{\kappa}$$

$$T_{max} = a \cdot T_C \cdot \delta$$

$$b = 1 + \frac{(1 - \psi - \theta) \cdot \delta}{\kappa \cdot \left(\varepsilon_c^{\,\kappa-1} + \psi \cdot \delta\right)}$$

$$\eta_{th} = \frac{1}{\delta} \cdot \left[1 - \varepsilon_c^{\,\kappa-1} + \frac{\kappa-1}{\kappa} \cdot (1 - \psi) \cdot \delta + \frac{\theta \cdot \delta}{\kappa} \dots \right. \dots$$
$$\left. + \frac{\kappa-1}{\varepsilon_c} \cdot \left[\varepsilon_c - 1 - \phi \cdot (\varepsilon_e - 1)\right]\right]$$
$$+ a \cdot \left[1 - \left(\frac{b}{\varepsilon_e}\right)^{\kappa-1} \cdot \exp\left(\frac{\theta}{a}\right)\right]$$

Formula for the ideal V,p,T-model

$$T_4 = T_{max} \cdot \left[\frac{a \cdot \delta}{\varepsilon_e \cdot \left(\varepsilon_c^{\,\kappa-1} + \psi \cdot \delta\right)}\right]^{\kappa-1} \cdot \exp\left(\frac{\theta}{a}\right)$$

$$T_T = T_4 \cdot \left(\frac{p_T}{p_C} \cdot \frac{T_C}{T_4} \cdot \frac{\varepsilon_e}{\varepsilon_c}\right)^{\frac{\kappa-1}{\kappa}}$$

$$p_4 = p_C \cdot \frac{T_4}{T_C} \cdot \frac{\varepsilon_c}{\varepsilon_e}$$

$$p_T = p_u + \frac{p_4 - p_u}{10} \quad \text{(hypothetical)}$$

$$W_{TTu} = \eta_{sT} \cdot (m_a + m_f) \cdot c^\circ_p \cdot T_T \cdot \left(1 - \frac{T_u}{T_T}\right)$$

$$W_{CuC} = \frac{m_a \cdot c^\circ_p \cdot T_u}{\eta_{sC}} \cdot \left[\left(\frac{p_C}{p_u}\right)^{\frac{\kappa-1}{\kappa}} - 1\right]$$

Requirements for cycle realization

1. Requirement (for maximal pressure)

$$p_{max} \geq p_C \cdot \varepsilon_c^{\,\kappa} \qquad \text{i.e.} \qquad \psi \geq 0$$
$$p_{max} \leq p_C \cdot \varepsilon_c \cdot \left(\varepsilon_c^{\,\kappa-1} + \delta\right)$$

2. Requirement (for maximal temperature)

$$T_{max} \geq T_C \cdot \varepsilon_c^{\,\kappa-1}$$
$$T_{max} \leq T_C \cdot \left(\varepsilon_c^{\,\kappa-1} + \psi \cdot \delta + \frac{\delta}{\kappa}\right)$$

3. Requirement (for heat release)

$$1 - \psi - \theta \geq 0 \qquad \text{and} \qquad \theta \geq 0$$

4. Requirement (for expansion)

$$p_4 > p_u$$

5. Requirement (for turbocharging)

$$W_{TTu} > W_{CuC}$$
$$p_T > p_u$$